Available online at www.sciencedirect.com
ScienceDirect
Trans. Nonferrous Met. Soc. China 28(2018) 1828−1837
Transactions of Nonferrous Metals Society of China
www.tnmsc.cn

Hydrogen storage performances of as-milled $REMg_{11}Ni$ (RE=Y, Sm) alloys catalyzed by MoS_2

Yang-huan ZHANG[1,2], Wei ZHANG[1,2], Ze-ming YUAN[1,2], Wen-gang BU[2], Yan QI[2], Xiao-ping DONG[3], Shi-hai GUO[2]

1. Key Laboratory of Integrated Exploitation of Baiyun Obo Multi-Metal Resources, Inner Mongolia University of Science and Technology, Baotou 014010, China;
2. Department of Functional Material Research, Central Iron and Steel Research Institute, Beijing 100081, China;
3. Department of Mechanical Engineering, Hebei University, Baoding 071002, China

Received 1 June 2017; accepted 30 September 2017

Abstract: To compare the hydrogen storage performances of as-milled $REMg_{11}Ni-5MoS_2$ (mass fraction) (RE=Y, Sm) alloys, which were catalyzed by MoS_2, the corresponding alloys were prepared. The hydrogen storage performaces of these alloys were measured by various methods, such as XRD, TEM, automatic Sievert apparatus, TG and DSC. The results reveal that both of the as-milled alloys exhibit a nanocrystalline and amorphous structure. The RE=Y alloy shows a larger hydrogen absorption capacity, faster hydriding rate, lower initial hydrogen desorption temperature, superior hydrogen desorption property, and lower hydrogen desorption activation energy, which is thought to be the reason of its better hydrogen storage kinetics, as compared with RE=Sm alloy.
Key words: Mg-based alloy; ball milling; catalyst; rare earth element; hydrogen storage performance

1 Introduction

As is well known, the end of the Stone Age is not because of the depletion of stone. Likewise, the termination of the fossil fuel era does not need to wait until it dries up. In other words, human beings cannot be forced to abandon the car due to the exhaustion of fossil fuels; instead, mankind is very likely to initiatively give up fossil fuels in the case of the great development of automobile. Hydrogen is considered to be the best fuel for fuel cells owing to its outstanding versatility, utilization efficiency, safety, environment compatibility and inexhaustible reserves [1−3]. However, hydrogen storage is the major technology barrier to the introduction of hydrogen economy [4,5]. That is to say, the schedule of acclaiming hydrogen fuel cell vehicle as a wide commercial application of the 21st century will principally depend on hydrogen storage technology [6]. Metal hydride hydrogen storage, one of hydrogen storage methods, is regarded to be the most promising alternative to satisfy the requirements for mobile application [4]. Mg and Mg-based alloys, as promising hydrogen storage materials, have been extensively investigated [7−9] due to some of their unique advantages, such as high gravimetric (7.6%, mass fraction) and volumetric (110 kg/m^3) hydrogen storage densities, good reversibility in de-/hydrogenation processes and low cost [10]. However, some of their disadvantages, such as the relatively high thermal stability and slow de-/hydrogenation kinetics, impede their commercial application in hybrid electric vehicle [11]. Therefore, the hydrogen storage thermodynamics and kinetics of Mg and Mg-based alloys need to be further ameliorated.

It has been ascertained that the change of structures can dramatically affect the de-/hydrogenation thermodynamics and kinetics of Mg and Mg-based alloys [12,13]. Especially, reducing the grain size of Mg-based alloys far below micron size can significantly ameliorate their de-/hydrogenation characteristics [14]. Mechanical milling [15,16] and melt spinning [17] are generally accepted as two commonly used strategies for obtaining nanostructure and ameliorating hydrogen storage performance. However, whether ball mill can improve hydrogen storage thermodynamics is still a questionable issue. LASS [18] considered that ball milling, in theory, can improve the thermodynamics of de-/hydrogenation reactions by introducing capillarity

Foundation item: Projects (51761032, 51471054, 51871125) supported by the National Natural Science Foundation of China
Corresponding author: Yang-huan ZHANG; Tel: +86-10-62183115; Fax: +86-10-62187102; E-mail: zhangyh59@sina.com
DOI: 10.1016/S1003-6326(18)64827-7

effects when particle size is reduced to a small enough size. While AGARWAL et al [19] stated that ameliorating thermodynamics by ball milling is possible only when the particle size is less than 5 nm, which has not yet been achieved by using mechanical milling for now.

Furthermore, it was confirmed that the dissociation of hydrogen molecules on Mg surface requires a fairly large energy (1.15 eV), which is the rate controlling factor for the hydrogenation of Mg. Catalysts may reduce this dissociation energy for hydrogen storage in Mg. For example, the addition of transition metals Pd, Cu, Ni and Co can reduce it to 0.39, 0.56, 0.06, and 0.03 eV, respectively [20]. It was proven that the partial substitution of rare earth elements (La, Ce, Pr, Nd, Y, Sm) for Mg [21−23] and the addition of transition metals (Ni, Ti, V, Fe, Cu) considerably ameliorate the thermodynamics of de-/hydrogenation [20,24,25]. Theoretically, the substitutional atoms in MgH_2 can weaken Mg—H bond through interactions between the valance electron of H and the unsaturated d/f electron shells of transition metals as catalyst, and thus the desorption behavior of MgH_2 can be ameliorated greatly [26]. Generally, rare earth elements [23], transition metallic elements [27] as well as their oxides [28], fluorides [29], halides [7], hydrides [21] and intermetallic compounds [19] are verified to be good catalysts which can destabilize MgH_2 and enhance the de-/hydriding rate of alloy hydrides. SADHASIVAM et al [14] investigated the effect of adding Mm (Ce and La as the dominant components) oxide on hydrogen desorption kinetics of MgH_2 and the results revealed that Mm-oxide is an effective catalyst for improving the hydrogen sorption behavior of MgH_2. The initial desorption temperature for 5% (mass fraction) Mm-oxide catalyzed MgH_2 was decreased from 654 (ball-milled) to 578 K, viz. a decrease by 76 K. DARYANI et al [30] reported that adding catalyst TiO_2 can significantly enhance the milling efficiency and accelerate the size reduction of MgH_2 during ball milling. Moreover, the addition of 6% (molar fraction) TiO_2 markedly improved the hydrogen absorption kinetics and made the decomposition temperature of as-milled MgH_2 decreased by 100 K. MoS_2 is a naturally occurring layered solid and has been widely used as dry lubricant and catalyst [31−33]. WANG et al [34] have added MoS_2 into $2LiBH_4$−MgH_2 system as catalyst, which showed a good catalysis in both de-/hydrogenation kinetics and thermodynamics. HUANG et al [35] studied the catalysis of Mo, MoO_2, MoO_3 and MoS_2 in catalyzing the hydrolysis of Mg composites in seawater, one of the promising hydrogen generation technologies, and got a good outcome.

In the present work, a trace of MoS_2 was added into the alloys. According to the recent result made by EL-ESKANDARANY et al [36], 5% (mass fraction) is thought to be the optimum amount of added MoS_2. Ball milling technology has been utilized to synthesize $REMg_{11}Ni$−$5MoS_2$ (RE=Y, Sm) alloys. A comparison of structure and hydrogen storage performance of the as-milled alloys containing different rare earth elements was performed.

2 Experimental

The $REMg_{11}Ni$ (RE=Y, Sm) alloy ingots were synthesized in a vacuum induction furnace under the protective atmosphere of helium to prevent the evaporation of Mg element. Prior to testing de-/hydriding performances, experimental samples were mechanically pulverized into powders of about 50 μm in diameter, and then 5% (mass fraction) MoS_2 was added into the alloy powder. The hardened steel balls (210 g) and mixed powder (6 g) were homogeneously mixed under argon protection in Cr−Ni stainless steel vials. The mechanical mill is a planetary-type mill with 135 r/min of disc revolution speed. In each cycle, 50 min milling and 10 min resting were programmed with a total milling time of 20 h. The experimental samples were treated in an Ar-filled glove box to avoid contaminating.

The X-ray diffraction patterns after milling were obtained by an X-ray diffractometer (XRD) (D/max-2400) with Cu $K_{\alpha 1}$ radiation. The scan rate is 10 (°)/min. The microstructure and crystalline states of alloys dealt by milling were characterized by a high resolution transmission electron microscope (HRTEM) (JEM−2100F, operated at 200 kV) and electron diffraction (ED).

The isothermal de-/hydriding kinetics was performed on an automatically Sieverts apparatus. The hydrogenation performance was measured at 593, 613, 633 and 653 K under 3 MPa H_2, while the dehydrogenation performance was conducted at the same temperature under 1×10^{-4} MPa. In each experiment, the stainless steel reactor needs to be sealed with 300 mg sample powder in it. Thermogravimetry (TG) and differential scanning calorimetry (DSC) (SDT-Q600) were adopted to investigate the non-isothermal dehydrogenation performance. The heating runs were performed at different rates (5, 10, 15 and 20 K/min). The test sample mass was typically 20 mg.

3 Results and discussion

3.1 Microstructure characteristics

The XRD diffraction patterns of as-milled $REMg_{11}Ni$−$5MoS_2$ (RE=Y, Sm) alloys before and after de-/hydrogenation are presented in Fig. 1. The hydrogenation reaction was performed at 593 K and

3 MPa, and dehydrogenation reaction at 593 K and 1×10^{-4} MPa. It is found that adding catalyst MoS_2 does not create any new phase in the patterns, implying that there is no reaction between MoS_2 and any element in the alloy. The ICDD identification of XRD patterns reveals that the as-cast RE=Y alloy (not present here) includes major phase $Mg_{24}Y_5$ and secondary phase Mg_2Ni, while RE=Sm alloy contains major phase Sm_5Mg_{41} and secondary phases $SmMg_3$ and Mg_2Ni. Mechanical milling makes diffraction peaks merge and broadened dramatically, showing a typical nanocrystalline and amorphous structure. After being hydrogenated, the alloy exhibits an obvious crystalline reaction, and three hydrides can be found in RE=Y alloy, viz. MgH_2, Mg_2NiH_4 and YH_3. Based on XRD analysis, possible formation pathways of the hydrides can be inferred as follows [37]:

$$Mg_{25}Y_5+H_2 \rightarrow MgH_2+YH_2 \quad (1)$$

$$YH_2+H_2 \rightarrow YH_3 \quad (2)$$

$$Mg_2Ni+H_2 \rightarrow Mg_2NiH_4 \quad (3)$$

But for RE=Sm alloy, the hydride phases are MgH_2, Mg_2NiH_4 and Sm_3H_7. The possible formation pathways of these hydrides can be inferred as follows [38]:

$$Sm_5Mg_{41}+H_2 \rightarrow MgH_2+Sm_3H_7 \quad (4)$$

$$SmMg_3+H_2 \rightarrow MgH_2+Sm_3H_7 \quad (5)$$

$$Mg_2Ni+H_2 \rightarrow Mg_2NiH_4 \quad (6)$$

It can be seen from Fig. 1(a) that three phases appear in dehydrogenated RE=Y alloy, including YH_2, Mg and Mg_2Ni. The path of the dehydrogenation reactions can be inferred as follows:

$$MgH_2 \rightarrow Mg+H_2 \quad (7)$$

$$Mg_2NiH_4 \rightarrow Mg_2Ni+H_2 \quad (8)$$

$$YH_3 \rightarrow YH_2+H_2 \quad (9)$$

It is evident that the YH_2 phase keeps undecomposed, which is assigned to its high thermal stability. Meanwhile, three phases appear in dehydrogenated RE=Sm alloy, including Sm_3H_7, Mg and Mg_2Ni, as seen from Fig. 1(b). The path of these dehydrogenation reactions can be drawn as follows:

$$MgH_2 \rightarrow Mg+H_2 \quad (10)$$

$$Mg_2NiH_4 \rightarrow Mg_2Ni+H_2 \quad (11)$$

Apparently, the Sm_2H_7 phase keeps unchanged, which is assigned to its high thermal stability. It can be found that the reversible hydriding and dehydriding cycles of the activated RE=Y alloy include the following reactions:

$$Mg+H_2 \rightleftharpoons MgH_2 \quad (12)$$

$$Mg_2Ni+H_2 \rightleftharpoons Mg_2NiH_4 \quad (13)$$

$$YH_2+H_2 \rightleftharpoons YH_3 \quad (14)$$

And for RE=Sm alloy, the reversible cycles include the following reactions:

$$Mg+H_2 \rightleftharpoons MgH_2 \quad (15)$$

$$Mg_2Ni+H_2 \rightleftharpoons Mg_2NiH_4 \quad (16)$$

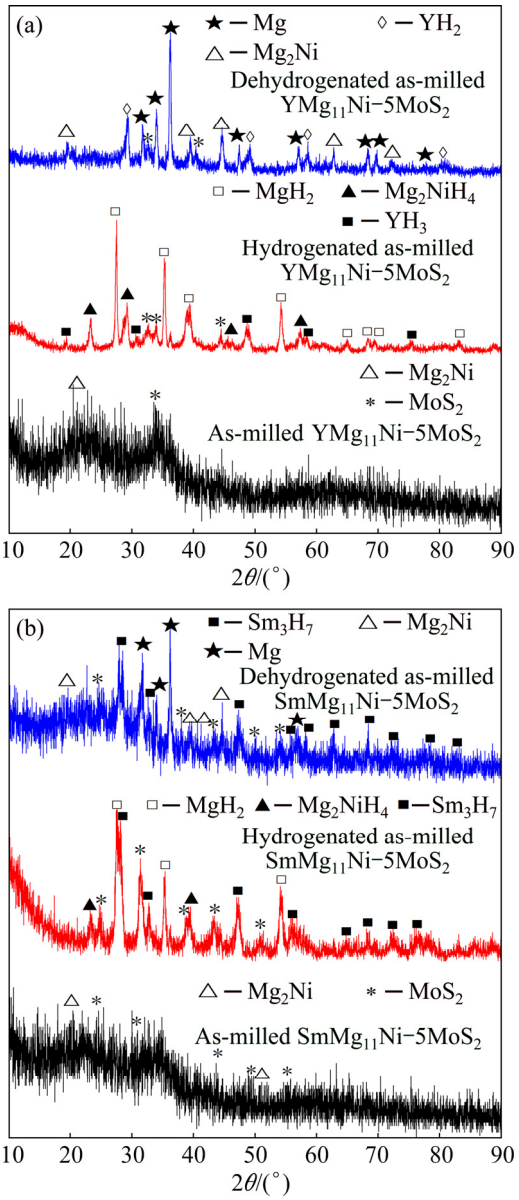

Fig. 1 XRD patterns of as-milled $REMg_{11}Ni-5MoS_2$ (RE=Y, Sm) alloys before and after hydrogen absorption and desorption: (a) RE=Y; (b) RE=Sm

Figure 2 shows the microstructure and crystalline states of as-milled $REMg_{11}Ni-5MoS_2$ (RE=Y, Sm) alloys before and after hydrogen absorption and desorption. According to the HRTEM and ED analyses, a nanocrystalline and amorphous structure is observed. Furthermore, measured by linear intercept method, the average grain size is gauged to be 20 nm. The MoS_2

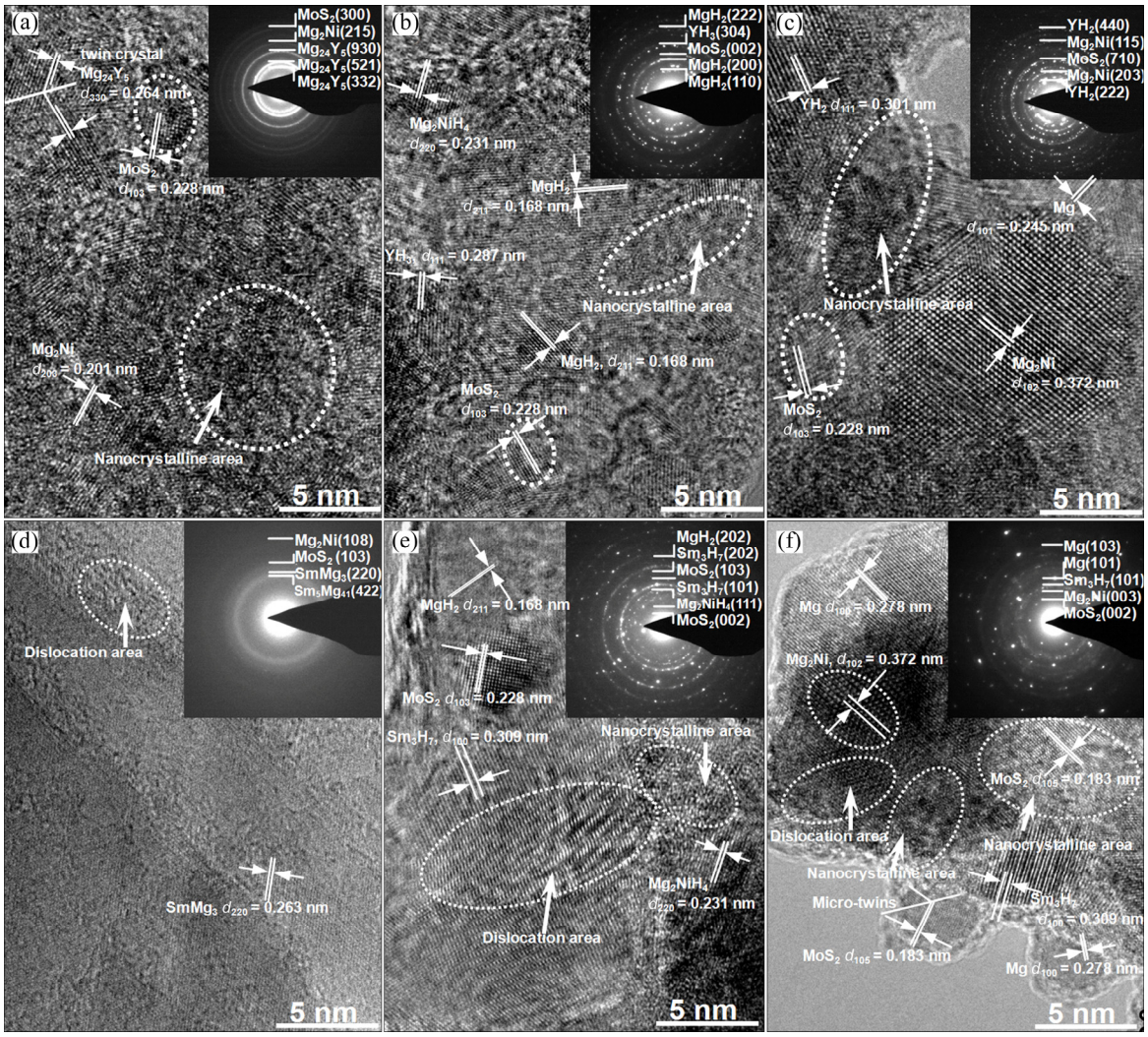

Fig. 2 HRTEM micrographs and SAD patterns of as-milled alloys in different states: (a) As-milled $YMg_{11}Ni-5MoS_2$; (b) Hydrogenated $YMg_{11}Ni-5MoS_2$; (c) Dehydrogenated $YMg_{11}Ni-5MoS_2$; (d) As-milled $SmMg_{11}Ni-5MoS_2$; (e) Hydrogenated $SmMg_{11}Ni-5MoS_2$; (f) Dehydrogenated $SmMg_{11}Ni-5MoS_2$

additive does not change the phase composition of $REMg_{11}Ni$ (RE=Y, Sm) alloys, containing $Mg_{24}Y_5$ and Mg_2Ni phases in RE=Y alloy and Sm_5Mg_{41}, Mg_2Ni and $SmMg_3$ phases in RE=Sm alloy, which is also evidenced by the analysis of ED patterns. After being hydrogenated, the amount of the amorphous phase of as-milled $REMg_{11}Ni$ (RE=Y, Sm) alloys obviously decreases, although the nanocrystalline and amorphous structure (Figs. 2(b) and (d)) still exists. This indicates that hydrogen absorption facilitates crystalline reaction. Three hydrides, MgH_2, Mg_2NiH_4 and YH_3, appear in hydrogenated RE=Y alloy, and MgH_2, Mg_2NiH_4 and Sm_3H_7 appear in hydrogenated RE=Sm alloy, which are supported by ED patterns. It is found from Figs. 2(c) and 2(f) that dehydrogenated $REMg_{11}Ni$ (RE=Y, Sm) alloys both have a completely crystalline structure, and the grain sizes grow visibly. A similar result was reported by PUKAZHSELVAN et al [15]. The structural analysis and the index of ED rings of alloys reveal that there are three phases in dehydrogenated RE=Y alloy, viz. Mg, Mg_2Ni and YH_2 and three phases Mg, Mg_2Ni and Sm_3H_7 in dehydrogenated RE=Sm alloy. Apparently, YH_2 and Sm_3H_7 maintain undecomposed in the process of hydrogen desorption, which is consistent with XRD detections.

3.2 Hydrogen absorption and desorption kinetics

The non-isothermal dehydrogenation performance of as-milled $REMg_{11}Ni-5MoS_2$ (RE=Y, Sm) alloys was investigated by thermogravimetry (TG). The temperature programmed desorption curve of the alloys by saturated hydriding at 593 K and 3 MPa, are illustrated in Fig. 3 at a heating rate of 5 K/min. In order to avoid the effect of desorption temperature due to incremental pressure, the mass of sample is set equal in each closed chamber. It is found that the as-milled $REMg_{11}Ni-5MoS_2$ (RE=Y, Sm)

alloys start to release hydrogen at about 525.8 and 545.7 K, respectively. This suggests that the change of rare earth elements affects the initial desorption temperature of alloy, which might be ascribed to the weakened Mg — H bond caused by the electronic exchange reaction between rare earth elements and MgH_2. Lower initial desorption temperature of RE=Y alloy means that its Mg—H bond is weakened more seriously.

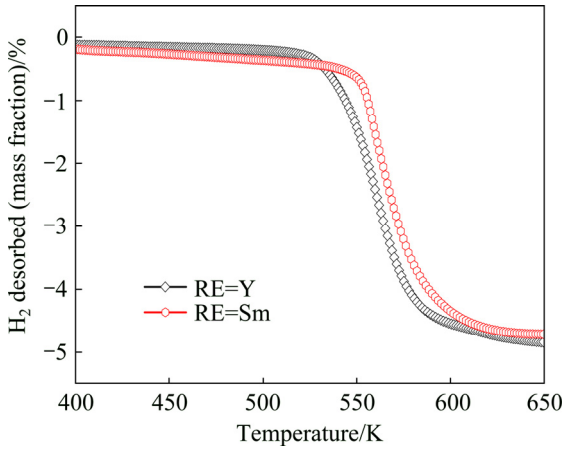

Fig. 3 Temperature programmed desorption curves of as-milled $REMg_{11}Ni$−$5MoS_2$ (RE=Y, Sm) alloys after hydrogen absorption at heating rate of 5 K/min

To inspect the different influences of elements Y and Sm on hydriding kinetics, the variations of hydriding capacity of as-milled $REMg_{11}Ni$−$5MoS_2$ (RE=Y, Sm) alloys with hydriding reaction time were operated at 593, 613, 633 and 653 K and 3 MPa. A rapid hydriding rate exhibits in the first few minutes, after which the value of hydrogen absorption capacity increases tardily at a long hydriding time, and the maximal hydrogenation capacity is nearly saturated, as shown in Fig. 4. These hydrogenation curve characteristics are most likely determined by the fact that within the first few minutes a surface-near hydride layer is formed, so that the diffusion of hydrogen through this layer becomes a rate-limiting factor. For facilitating comparison, 60 s is taken as a reference of hydrogen absorption time. It can be derived from Fig. 4 that the hydrogen absorption capacities within 60 s at 593, 613, 633 and 653 K are 4.363%, 4.577%, 4.708% and 4.827% (mass fraction), respectively, for RE=Y alloy, and 4.233%, 4.481%, 4.520% and 4.674% (mass fraction) for RE=Sm alloy. Apparently, the hydrogen absorption capacity for the fixed time is in order of RE=Y>RE=Sm, meaning that the element Y can facilitate the hydriding kinetics more than element Sm. It has been well known that hydrogenation process of MgH_2 is dominated by three critical steps, namely, 1) H_2 molecules decomposing into H atoms on the surface of alloy, 2) H atoms diffusing along grain boundaries, and 3) hydrogenation of Mg atoms and transforming into MgH_2 molecules. It is convinced that the decomposing energy of H_2 molecules is fairly high, which considerably dominates the hydriding rate of Mg [39]. POURABDOLI et al [40] considered that the addition of rare earth elements or their oxides may reduce dissociation energy and thus can be used as catalysts for hydrogen storage in Mg. Thereby, it is well-founded to believe that the addition of Y or Sm particles facilitates step 1), i.e., the dissociation of hydrogen molecules into atoms, and the addition of Y has a better improvement.

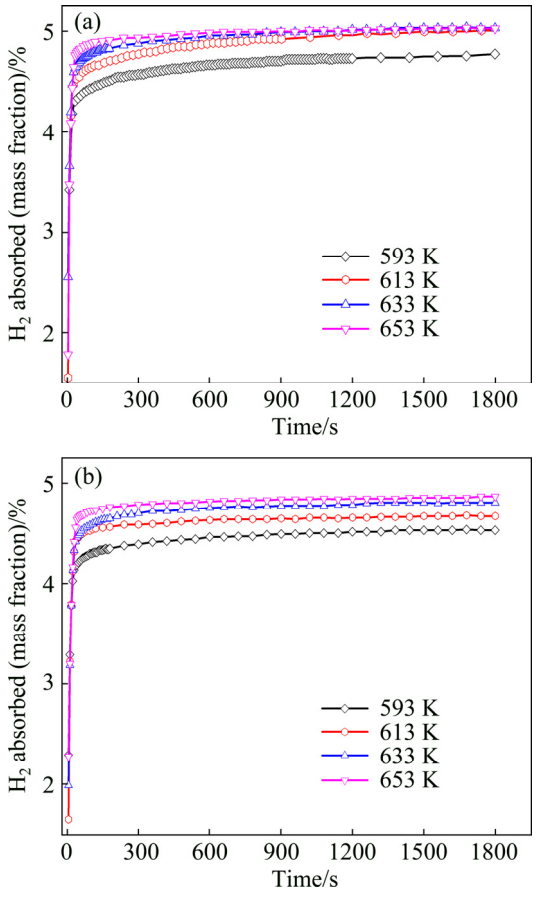

Fig. 4 Hydrogen absorption kinetic curves of as-milled $REMg_{11}Ni$−$5MoS_2$ (RE=Y, Sm) alloys at different temperatures: (a) RE=Y; (b) RE=Sm

To investigate the effect of different rare earth elements on hydrogen desorption kinetics, isothermal dehydrogenation measurements of as-milled $REMg_{11}Ni$−$5MoS_2$ (RE=Y, Sm) alloys were conducted at different temperatures, as illustrated in Fig. 5. The isothermal dehydrogenation curves of as-milled alloys were studied at 593, 613, 633, and 653 K. Distinctly, the temperature change causes a significant influence on dehydrogenation kinetics. The rise of temperature markedly enhances the dehydriding rate of alloys. It can be derived from Fig. 5 that the time needed by desorbing 3% (mass

fraction) H_2 at 593, 613, 633 and 653 K is 507, 208, 125 and 86 s, respectively, for RE=Y alloy, and 938, 586, 296 and 140 s for RE=Sm alloy. This indicates that the variation of rare earth elements has a significant effect on improving the dehydrogenation kinetics of $REMg_{11}Ni-5MoS_2$ (RE=Y, Sm) alloys. Obviously, the hydrogen desorption capacity for the fixed time is in order of RE=Y>RE=Sm, indicating that the hydrogen desorption kinetics can be improved more seriously by the addition of rare earth element Y.

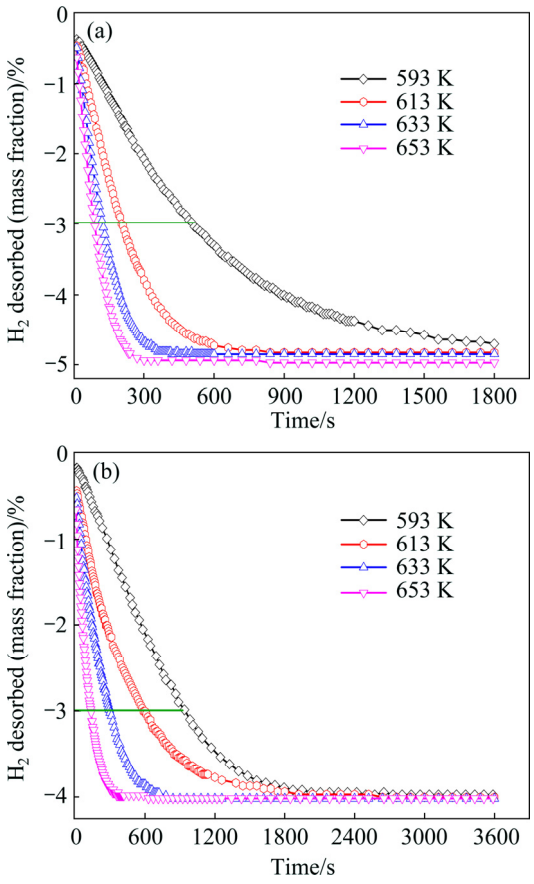

Fig. 5 Hydrogen desorption kinetic curves of as-milled $REMg_{11}Ni-5MoS_2$ (RE=Y, Sm) alloys at different temperatures: (a) RE=Y; (b) RE=Sm

3.3 Dehydrogenation activation energy

To understand the mechanism of RE=Y alloy possessing a faster dehydriding rate as compared with RE=Sm alloy, the dehydrogenation activation energy is estimated by Arrhenius and Kissinger methods for $REMg_{11}Ni-5MoS_2$ (RE=Y, Sm) alloys due to the fact that the energy barrier for MgH_2 releasing H_2 is deemed to be a dominated factor for dehydrogenation kinetics. Generally, the total energy barrier, which must be overcome in a gas−solid reaction, is signified by dehydrogenation activation energy. It is well known that the hydrogen desorption reaction is completed through a nucleation and growth process. Usually, the nucleation and growth process taking place during hydrogen desorption can be simulated by Johnsone−Mehle−Avramie (JMA) model, which can be expressed by the following equation [40]:

$$\ln[-\ln(1-\alpha)] = \eta \ln k + \eta \ln t \quad (17)$$

where α is the reaction rate of MgH_2 transforming into Mg at time t, k is an effective kinetic parameter and η is the reaction order or Avrami exponent. The JMA graphs of $\ln[-\ln(1-\alpha)]$ vs $\ln t$ at 593, 613, 633 and 653 K can be constructed by using logarithmic transform of Eq. (17), as presented in Fig. 6. The JMA plots are found to be nearly linear, implying that the dehydriding reaction of alloys starts from an instantaneous nucleation followed by interface controlled three-dimensional growth process [41]. Thus, the η and $\eta \ln k$ values at different temperatures can be derived from the slope and intercept of JMA plots and the rate constant k can be easily calculated. The dehydrogenation activation energy (E_a^{de}) can be evaluated from Arrhenius equation [42]:

$$k = A\exp\left(\frac{-E_a^{de}}{RT}\right) \quad (18)$$

where A and R are the pre-exponential factor and gas constant, respectively.

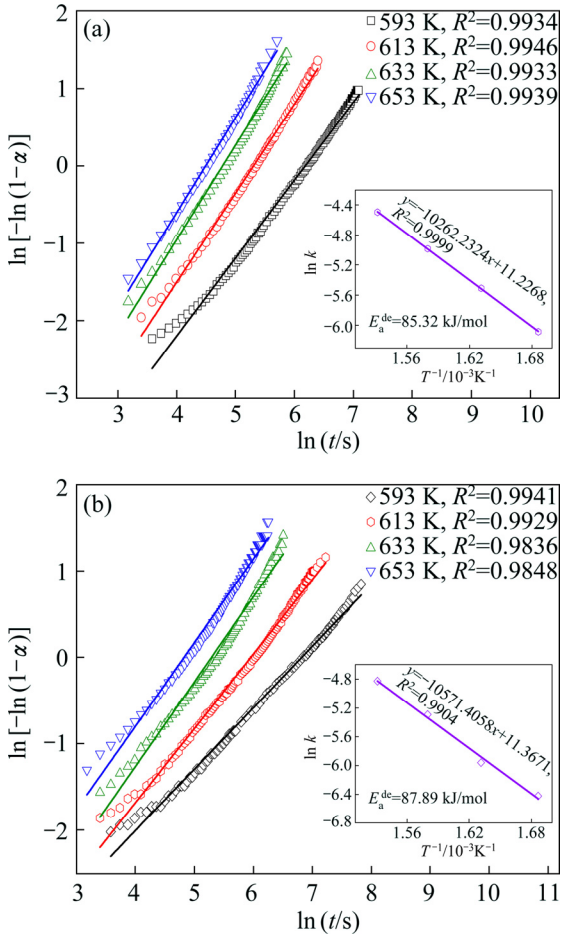

Fig. 6 JMA graphs and Arrhenius plots of as-milled $REMg_{11}Ni-5MoS_2$ (RE=Y, Sm) alloys: (a) RE=Y; (b) RE=Sm

The Arrhenius plots of $\ln k$ vs $1/T$ for dehydrogenation process are given in Fig. 6. Therefore, the activation energy E_a^{de} can be derived from the slopes. The E_a^{de} values are 85.32 and 87.89 kJ/mol for RE=Y and RE=Sm alloys, viz. a reduction by 2.57 kJ/mol in activation energy.

Here, Kissinger method is also used to evaluate the dehydrogenation activation energy E_k^{de} for comparison. Kissinger equation is as follows [43]:

$$\frac{\mathrm{d}[\ln(\beta/T_P^2)]}{\mathrm{d}(1/T_P)}=\frac{-E_k^{de}}{R} \tag{19}$$

where T_P is thermodynamic temperature, R is mole gas constant and β is heating rate.

The DSC curves of hydrogenated $REMg_{11}Ni-5MoS_2$ (RE=Y, Sm) alloys under different heating rates were measured to determine the dehydrogenation activation energy E_k^{de}. As displayed in Fig. 7, a dehydrogenated endothermic peak is obviously seen, and the peak shapes are similar for all alloys, indicating that the reaction processes are same. Additionally, for RE=Y alloy, the endothermic peak shows a drift tendency to low temperature, suggesting that element Y can also improve the dehydrogenation reaction rate. Based on the data in Fig. 7, the graphs of $\ln(\beta/T_P^2)$ vs $1/T_P$ can be built by using logarithmic transform of Eq. (19), which is termed as Kissinger plots, as inserted in Fig. 7. The Kissinger plots are found to be nearly linear, and thus the activation energy E_k^{de} can be easily calculated from the slopes of the fitting line. The E_k^{de} values of $REMg_{11}Ni-5MoS_2$ (RE=Y, Sm) alloys are 77.58 and 82.62 kJ/mol, respectively. Obviously, the activation energy evaluated from Arrhenius equation is larger compared with that from Kissinger equation. BARICCO et al [44] reported a similar result. Furthermore, it has a same result that the activation energy of RE=Y alloy is always lower than that of RE=Sm alloy, whichever method is used. Thereby, a conclusion can be drawn that the decrease of dehydrogenation activation energy is the real driving force for ameliorating dehydrogenation kinetics. FAN et al [45] considered that the activation energy (E_a) for hydrogen desorption is an important indicator to evaluate the dehydrogenation performance. The reduction of activation energy E_a means that the energy barriers of hydrogen releasing from the system are reduced.

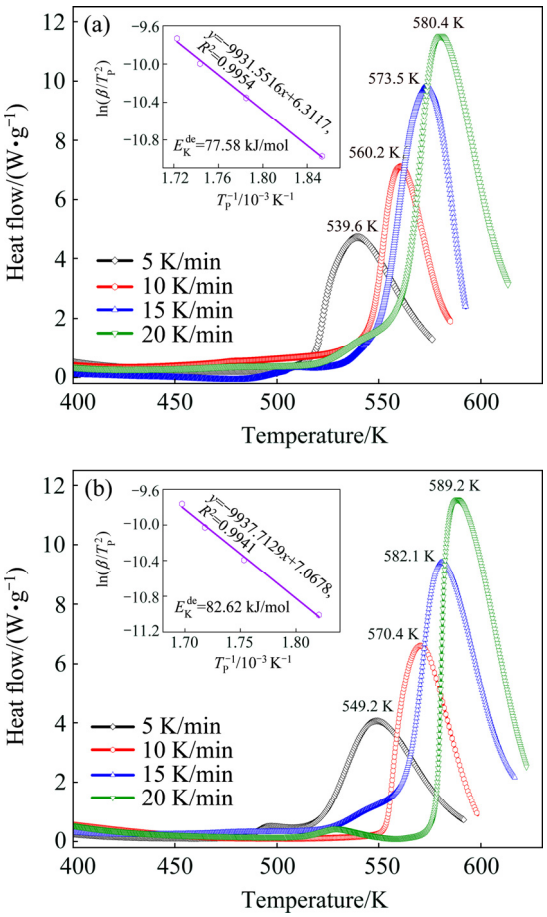

Fig. 7 DSC curves and Kissinger plots of as-milled $REMg_{11}Ni-5MoS_2$ (RE=Y, Sm) alloys at various heating rates: (a) RE=Y; (b) RE=Sm

3.4 *P*−*C*−*T* curves and hydrogen storage thermodynamics

To inspect the different effects of elements Sm and Y on de-/hydrogenation thermodynamics, *P*−*C*−*T* curves are measured at 593, 613, 633 and 653 K for the as-milled $REMg_{11}Ni-5MoS_2$ (RE=Y, Sm) alloys. It is presented in Fig. 8 that the absorption and desorption pressure plateaus are fairly flat and the hysteresis ($H_f=\ln(P_a/P_d)$) is quite small. The variations of rare earth elements have an insignificant effect on the plateau features of *P*−*C*−*T* curves. It is clear that each *P*−*C*−*T* curve has two pressure plateaus. Among them, the lower pressure corresponds to the formation and dissociation of MgH_2, while the higher one corresponds to Mg_2NiH_4. Based on the plateau pressures (P_a and P_d) in Fig. 8, thermodynamics parameters, viz. enthalpy ΔH and entropy ΔS, can be derived from Van't Hoff equation [46]:

$$\ln\left(\frac{P_{H_2}}{P_0}\right)=\frac{\Delta H}{RT}-\frac{\Delta S}{R} \tag{20}$$

where P_0 is 1.01325×10^5 Pa, R is the mole gas constant and P_{H_2} is the equilibrium plateau pressure corresponding to MgH_2. The van't Hoff graphs of $\ln P_{H_2}/P_0$ vs $1/T$ for as-milled $REMg_{11}Ni-5MoS_2$ (RE=Y, Sm) alloys can be plotted by using logarithmic transform of Eq. (20), as inserted in Fig. 8. According to the slopes and intercepts of the fitting lines, the enthalpy ΔH and entropy ΔS can be easily calculated, as summarized in Table 1. This indicates that the substitution of Y for Sm renders a slight improvement on

hydrogen storage thermodynamics of the alloy as the absolute values of both ΔH and ΔS of RE=Y are a little smaller than those of RE=Sm alloy for both hydrogen absorption and desorption processes.

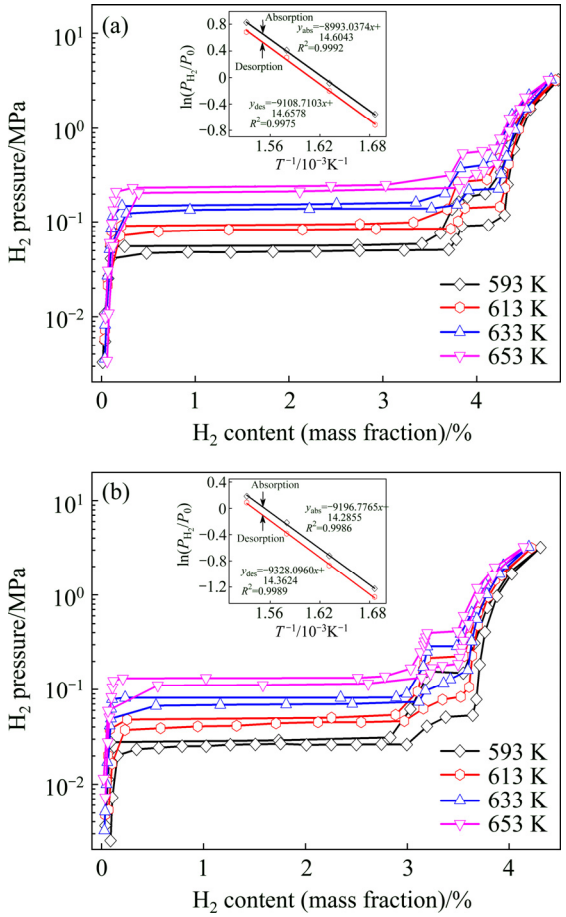

Fig. 8 *P*−*C*−*T* curves and van't Hoff plots of as-milled $REMg_{11}Ni$−$5MoS_2$ (RE=Y, Sm) alloys in temperature range of 593−653 K: (a) RE=Y; (b) RE=Sm

Table 1 Enthalpy ΔH and entropy ΔS of as-milled $REMg_{11}Ni$−$5MoS_2$ (RE=Y, Sm) alloys

Alloy	ΔH_{ab}/ (kJ·mol^{-1})	ΔS_{ab}/ (J·mol^{-1}·K^{-1})	ΔH_{de}/ (kJ·mol^{-1})	ΔS_{de}/ (J·mol^{-1}·K^{-1})
RE=Y	−74.76	−118.76	75.73	119.40
RE=Sm	−76.46	−121.42	77.55	121.86

4 Conclusions

1) The substitution of Y for Sm significantly improves the de-/hydriding rates of $REMg_{11}Ni$−$5MoS_2$ (RE=Y, Sm) alloys, for which the reduction of dehydrogenation activation energy produced by substituting Sm with Y is responsible.

2) The dehydrogenation activation energy is evaluated from Arrhenius and Kissinger equations. The results reveal that the dehydrogenation activation energy is visibly reduced by substituting Sm with Y, which is considered to be the real driving force of the dehydrogenation kinetics improved by substituting Sm with Y.

3) The substitution of Y for Sm incurs a slight reduction in enthalpy ΔH and entropy ΔS for the alloys. Furthermore, it facilitates to reduce the stability of alloy hydride. The initial hydrogen desorption temperature of hydrogenated $REMg_{11}Ni$−$5MoS_2$ (RE=Y, Sm) alloys is reduced from 545.7 to 525.8 K by substituting Sm with Y.

References

[1] JAIN I P. Hydrogen the fuel for 21st century [J]. International Journal of Hydrogen Energy, 2009, 34(17): 7368−7378.

[2] ZHANG Yang-huan, ZHAO Dong-liang, LI Bao-wei, QI Yan, GUO Shi-hai, WANG Xin-lin. Hydrogen storage behaviours of nanocrystalline and amorphous $Mg_{20}Ni_{10-x}Co_x$ (x=0−4) alloys prepared by melt spinning [J]. Transactions of Nonferrous Metals Society of China, 2010, 20(3): 405−411.

[3] ARUNACHALAM V S, FLEISCHER E L. The global energy landscape and materials innovation [J]. MRS Bulletin, 2008, 33(4): 264−288.

[4] SCHLAPBACH L, ZÜTTEL A. Hydrogen-storage materials for mobile applications [J]. Nature, 2001, 414(6861): 353−358.

[5] ZHANG Yang-huan, ZHANG Wei, SONG Xi-ping, ZHANG Pei-long, ZHU Yong-guo, QI Yan. Effects of spinning rate on structures and electrochemical hydrogen storage performances of RE−Mg−Ni−Mn-based AB_2-type alloys [J]. Transactions of Nonferrous Metals Society of China, 2016, 26(12): 3219−3231.

[6] WANG Hui, TAKENAKA S, OTSUKA K. Hydrogen storage properties of modified fumed-Fe-dust generated from a revolving furnace at a steel industry [J]. International Journal of Hydrogen Energy, 2006, 31(12): 1732−1746.

[7] MALKA I E, CZUJKO T, BYSTRZYCKI J. Catalytic effect of halide additives ball milled with magnesium hydride [J]. International Journal of Hydrogen Energy, 2010, 35(4): 1706−1712.

[8] ZHANG Yang-huan, LI Long-wen, FENG Dian-chen, GONG Peng-fei, SHANG Hong-wei, GUO Shi-hai. Hydrogen storage behavior of nanocrystalline and amorphous La−Mg−Ni-based $LaMg_{12}$-type alloys synthesized by mechanical milling [J]. Transactions of Nonferrous Metals Society of China, 2017, 27(3): 551−561.

[9] XU Chen-chen, XIAO Xue-zhang, SHAO Jie, LIU Lang-xia, QIN Teng, CHEN Li-xin. Effects of Ti-based additives on Mg_2FeH_6 dehydrogenation properties [J]. Transactions of Nonferrous Metals Society of China, 2016, 26(3): 791−798.

[10] ZHANG Yang-huan, XU Sheng, ZHAI Ting-ting, YANG Tai, YUAN Ze-ming, ZHAO Dong-liang. Hydrogen storage kinetics of nanocrystalline and amorphous Cu−Nd-added Mg_2Ni-type alloys [J]. Transactions of Nonferrous Metals Society of China, 2014, 24(11): 3524−3533.

[11] ZHAO Jun, CHEN Liang-jian, YU Kun, CHEN Chang, DAI Yi-long, QIAO Xue-yan, YAN Yang, YU Zhi-ming. Effects of chitosan coating on biocompatibility of Mg−6%Zn−10%$Ca_3(PO_4)_2$ implant [J]. Transactions of Nonferrous Metals Society of China, 2015, 25(3): 824−831.

[12] TERESIAK A, GEBERT A, SAVYAK M, UHLEMANN M, MICKEL C, MATTERN N. In situ high temperature XRD studies of the thermal behaviour of the rapidly quenched $Mg_{77}Ni_{18}Y_5$ alloy under hydrogen [J]. Journal of Alloys and Compounds, 2005, 398(1−2): 156−164.

[13] XIE Li-shuai, LI Jin-shan, ZHANG Tie-bang, KOU Hong-chao. Role of milling time and Ni content on dehydrogenation behavior of MgH_2/Ni composite [J]. Transactions of Nonferrous Metals Society of China, 2017, 27(3): 569−577.

[14] SADHASIVAM T, HUDSO M S L, PANDEY S K, BHATNAGAR A, SINGH M K, GURUNATHAN K, SRIVASTAVA O N. Effects of nano size mischmetal and its oxide on improving the hydrogen sorption behaviour of MgH_2 [J]. International Journal of Hydrogen Energy, 2013, 38(18): 7353−7362.

[15] PUKAZHSELVAN D, CAPURSO G, MADDALENA A, RUSSO S L, FAGG D P. Hydrogen storage characteristics of magnesium impregnated on the porous channels of activated charcoal scaffold [J]. International Journal of Hydrogen Energy, 2014, 39(35): 20045−20053.

[16] WANG Yao, ZENG Xiao-qin, ZOU Jian-xin, LI De-jiang, WU Xiao-mei, DING Wen-jiang. Microstructure characterization and hydrogen desorption behaviors of Mg−Al−H powders prepared by reactive milling in hydrogen [J]. Transactions of Nonferrous Metals Society of China, 2013, 23(10): 3112−3118.

[17] ZHANG Yang-huan, YANG Tai, BU Wen-gang, CAI Ying, ZHANG Guo-fang, ZHAO Dong-liang. Effect of Nd content on electrochemical performances of nanocrystalline and amorphous $(Mg_{24}Ni_{10}Cu_2)_{100-x}Nd_x$ (x=0−20) alloys prepared by melt spinning [J]. Transactions of Nonferrous Metals Society of China, 2013, 23(12): 3668−3676

[18] LASS E A. Hydrogen storage measurements in novel Mg-based nanostructured alloys produced via rapid solidification and devitrification [J]. International Journal of Hydrogen Energy, 2011, 36(17): 10787−10796.

[19] AGARWAL S, JAIN A, JAIN P, JANGIR M, VYAS D, JAIN I P. Effect of ZrCrCo alloy on hydrogen storage properties of Mg [J]. Journal of Alloys and Compounds, 2015, 645(S): s518−s523.

[20] POZZO M, ALFE D. Hydrogen dissociation and diffusion on transition metal (=Ti, Zr, Fe, V, Ru, Co, Rh, Ni, Pd, Cu, Ag) doped Mg (0001) surfaces [J]. International Journal of Hydrogen Energy, 2009, 34(4): 1922−1930.

[21] LUO F P, WANG H, OUYANG L Z, ZENG M Q, LIU J W, ZHU M. Enhanced reversible hydrogen storage properties of a Mg−In−Y ternary solid solution [J]. International Journal of Hydrogen Energy, 2013, 38(25): 10912−10918.

[22] KALINICHENKA S, RÖNTZSCH L, RIEDL T, WEISSGÄRBER T, KIEBACK B. Hydrogen storage properties and microstructure of melt-spun $Mg_{90}Ni_8RE_2$ (RE=Y, Nd, Gd) [J]. International Journal of Hydrogen Energy, 2011, 36(17): 10808−10815.

[23] ZOU Jian-xin, ZENG Xiao-qin, YING Yan-jun, CHEN Xi, GUO Hao, ZHOU Si, DING Wen-jiang. Study on the hydrogen storage properties of core-shell structured Mg−RE (RE=Nd, Gd, Er) nano-composites synthesized through arc plasma method [J]. International Journal of Hydrogen Energy, 2013, 38(5): 2337−2346.

[24] KNOTEK V, VOJTĚCH D. Electrochemical hydriding performance of Mg−TM−Mm (TM=transition metals, Mm=mischmetal) alloys for hydrogen storage [J]. Transactions of Nonferrous Metals Society of China, 2013, 23(7): 2047−2059.

[25] SONG Wen-jie, LI Jin-shan, ZHANG Tie-bang, HOU Xiao-jiang, KOU Hong-chao, XUE Xiang-yi, HU Rui. Microstructure and hydrogenation kinetics of Mg_2Ni-based alloys with addition of Nd, Zn and Ti [J]. Transactions of Nonferrous Metals Society of China, 2013, 23(12): 3677−3684.

[26] LIU Tong, ZHANG Tong-wen, ZHANG Xuan-zhuo, LI Xing-guo. Synthesis and hydrogen storage properties of ultrafine Mg−Zn particles [J]. International Journal of Hydrogen Energy, 2011, 36(5): 3515−3520.

[27] TANNIRU M, EBRAHIMI F. Effect of Al on the hydrogenation characteristics of nanocrystalline Mg powder [J]. International Journal of Hydrogen Energy, 2009, 34(18): 7714−7723.

[28] LONG Sheng, ZOU Jian-xin, CHEN Xi, ZENG Xiao-qin, DING Wen-jiang. A comparison study of Mg−Y_2O_3 and Mg−Y hydrogen storage composite powders prepared through arc plasma method [J]. Journal of Alloys and Compounds, 2014, 615(S): s684−s688.

[29] HOU Xiao-jiang, HU Rui, ZHANG Tie-bang, KOU Hong-chao, SONG Wen-jie, LI Jin-shan. Hydrogen desorption performance of high-energy ball milled Mg_2NiH_4 catalyzed by multi-walled carbon nanotubes coupling with TiF_3 [J]. International Journal of Hydrogen Energy, 2014, 39(34): 19672−19681.

[30] DARYANI M, SIMCHI A, SADATI M, HOSSEINI H M, TARGHOLIZADEH H, KHAKBIZ M. Effects of Ti-based catalysts on hydrogen desorption kinetics of nanostructured magnesium hydride [J]. International Journal of Hydrogen Energy, 2014, 39(36): 21007−21014.

[31] HE Zuo-li, QUE Wen-xiu. Molybdenum disulfide nanomaterials: Structures, properties, synthesis and recent progress on hydrogen evolution reaction [J]. Applied Materials Today, 2016, 3: 23−56.

[32] ZHANG Yang-huan, JI Meng, YUAN Ze-ming, BU Wen-gang, QI Yan, GUO Shi-hai. Catalytic effect of MoS_2 on hydrogen storage thermodynamics and kinetics of an as-milled $YMg_{11}Ni$ alloy [J]. RSC Advances, 2017, 7(60): 37689−37698.

[33] CHENG Ya-fei, LU Shun-kai, LIAO Fan, LIU Liang-bin, LI Yan-qing, SHAO Ming-wang. Rh-MoS_2 nanocomposite catalysts with Pt-like activity for hydrogen evolution reaction [J]. Advanced Functional Materials, 2017, 27(23): 1700359.

[34] WANG Jia-sheng, HAN Shu-min, ZHANG Wei, LIANG Dan, LI Yuan, ZHAO Xin, WANG Rui-bing. Effects of MoS_2 addition on the hydrogen storage properties of $2LiBH_4$–MgH_2 systems [J]. International Journal of Hydrogen Energy, 2013, 38(34): 14631−14637.

[35] HUANG Ming-hong, OUYANG Liu-zhang, YE Jian-shan, LIU Jiang-wen, YAO Xiang-dong, WANG Hui, SHAO Huai-yu, ZHU Min. Hydrogen generation via hydrolysis of magnesium with seawater using Mo, MoO_2, MoO_3 and MoS_2 as catalysts [J]. Journal of Materials Chemistry A, 2017, 5(18): 8566−8575.

[36] EL-ESKANDARANY M S, SHABAN E, AL-SHEMMIRI A. Integrated Ni/Nb_2O_5 nanocatalytic agent dose for improving the hydrogenation/dehydrogenation kinetics of reacted ball milled MgH_2 powders [J]. International Journal of Hydrogen Energy, 2014, 39(36): 21097−21106.

[37] YANG Tai, YUAN Ze-ming, BU Wen-gang, JIA Zhi-chao, QI Yan, ZHANG Yang-huan. Evolution of the phase structure and hydrogen storage thermodynamics and kinetics of $Mg_{88}Y_{12}$ binary alloy [J]. International Journal of Hydrogen Energy, 2016, 41(4): 2689−2699.

[38] YUAN Ze-ming, YANG Tai, BU Wen-gang, SHANG Hong-wei, QI Yan, ZHANG Yang-huan. Structure, hydrogen storage kinetics and thermodynamics of Mg-base Sm_5Mg_{41} alloy [J]. International Journal of Hydrogen Energy, 2016, 41(14): 5994−6003.

[39] SAKINTUNA B, DARKRIM F L, HIRSCHER M. Metal hydride materials for solid hydrogen storage: A review [J]. International Journal of Hydrogen Energy, 2007, 32(9): 1121−1140.

[40] POURABDOLI M, RAYGAN S, ABDIZADEH H, UNER D. Determination of kinetic parameters and hydrogen desorption characteristics of MgH_2−10 wt% (9Ni−2Mg−Y) nano-composite [J]. International Journal of Hydrogen Energy, 2013, 38(27): 11910−11919.

[41] CZUJKO T, VARIN R A, CHIU C, WRONSKI Z. Investigation of the hydrogen desorption properties of Mg + 10 wt.%X (X=V, Y, Zr) submicrocrystalline composites [J]. Journal of Alloys and Compounds, 2006, 414(1−2): 240−247.

[42] KIMURA T, MIYAOKA H, ICHIKAWA T, KOJIMA Y. Hydrogen absorption of catalyzed magnesium below room temperature [J]. International Journal of Hydrogen Energy, 2013, 38(31):

13728−13733.
[43] KISSINGER H E. Reaction kinetics in differential thermal analysis. [J]. Analytical Chemistry, 1957, 29(11): 1702−1706.
[44] BARICCO M, RAHMAN M W, LIVRAGHI S, CASTELLERO A, ENZO S, GIAMELLO E. Effects of $BaRuO_3$ addition on hydrogen desorption in MgH_2 [J]. Journal of Alloys and Compounds, 2012, 536(S): s216−s221.
[45] FAN Mei-qiang, LIU Shu-sheng, ZHANG Yao, ZHANG Jian, SUN Li-xian, XU Fen. Superior hydrogen storage properties of MgH_2−10 wt.% TiC composite [J]. Energy, 2010, 35(8): 3417−3421.
[46] FALAHATI H, BARZ D P J. Evaluation of hydrogen sorption models for AB_5-type metal alloys by employing a gravimetric technique [J]. International Journal of Hydrogen Energy, 2013, 38(21): 8838−8851.

MoS_2 催化的球磨态 $REMg_{11}Ni$ (RE=Y, Sm)合金的储氢性能

张羊换[1,2]，张 巍[1,2]，袁泽明[1,2]，卜文刚[2]，祁 焱[2]，董小平[3]，郭世海[2]

1. 内蒙古科技大学 内蒙古自治区白云鄂博矿多金属资源综合利用重点实验室，包头 014010；
2. 钢铁研究总院 功能材料研究所，北京 100081；
3. 河北大学 机械系，保定 071002

摘 要：制备 MoS_2 催化作用下的球磨态 $REMg_{11}Ni$−$5MoS_2$ (质量分数)(RE=Y, Sm)合金，用以比较其储氢性能。储氢性能通过多种方法测定，包括 XRD、TEM、自动 Sievert 设备、TG 和 DSC。结果显示，两种球磨态的合金都具有纳米晶和非晶结构。与 RE=Sm 合金相比，RE=Y 合金具有较大的吸氢量、较快的吸氢速率、较低的初始放氢温度、较好的放氢性能和较低的放氢活化能，其中较低的放氢活化能被视为其具备较好储氢动力学的原因。

关键词：镁基合金；球磨；催化剂；稀土元素；储氢性能

(Edited by Bing YANG)